Geophysical Research Letters

Supporting Information for

Overturning Pathways Control AMOC Weakening in CMIP6 Models

Baker J.A.[1], Bell M.J. [1], Jackson L.J. [1], Renshaw R. [1], Vallis G.K. [2], Watson A.J. [2], Wood R.A. [1]

[1] Met Office, UK.

[2] University of Exeter, UK.

Correspondence to: Jonathan Baker (jonathan.baker@metoffice.gov.uk)

Contents of this file

Model	Modeling Center	Ensemble member	Reference
ACCESS-CM2*	CSIRO-ARCCSS	r1i1p1f1	Bi et al. (2020)
ACCESS-ESM1-5*	CSIRO	r1i1p1f1	Ziehn et al. (2017, 2020)
CAS-ESM2-0*	CAS	r1i1p1f1	Zhang et al. (2020)
CESM2	NCAR	r1i1p1f1	Danabasoglu et al. (2020)
CESM2-FV2	NCAR	r1i1p1f1	Danabasoglu et al. (2020)
CESM2-WACCM*	NCAR	r1i1p1f1	Danabasoglu et al. (2020)
CESM2-WACCM-FV2	NCAR	r1i1p1f1	Danabasoglu et al. (2020)
CIESM	Tsinghua University	r1i1p1f1	Lin et al. (2020)
CMCC-CM2-HR4*	CMCC	r1i1p1f1	Cherchi et al. (2019)
CMCC-CM2-SR5*	CMCC	r1i1p1f1	Cherchi et al. (2019)
CMCC-ESM2	CMCC	r1i1p1f1	Lovato et al. (2022)
CNRM-CM6-1*	CNRM-CERFACS	r1i1p1f2	Voldoire et al. (2019)
CNRM-CM6-1-HR*	CNRM-CERFACS	r1i1p1f2	N/A
CNRM-ESM2-1*	CNRM-CERFACS	r1i1p1f2	Séférian et al. (2019)
CanESM5*	CCCma	r1i1p1f1	Swart et al. (2019)
E3SM-1-0	E3SM Project	r1i1p1f1	Golaz et al. (2019)
E3SM-1-1	E3SM Project	r1i1p1f1	Golaz et al. (2019)
E3SM-1-1-ECA	E3SM Project	r1i1p1f1	Golaz et al. (2019)
EC-Earth3	EC-Earth Consortium	r1i1p1f1	Wyser et al. (2020)
EC-Earth3-AerChem	EC-Earth Consortium	r1i1p1f1	Wyser et al. (2020)
EC-Earth3-CC	EC-Earth Consortium	r1i1p1f1	Wyser et al. (2020)
EC-Earth3-Veg	EC-Earth Consortium	r1i1p1f1	Wyser et al. (2020)
EC-Earth3-Veg-LR	EC-Earth Consortium	r1i1p1f1	Wyser et al. (2020)
FGOALS-f3-L*	CAS	r1i1p1f1	He et al. (2020)
FGOALS-g3*	CAS	r1i1p1f1	Li et al. (2020)
GFDL-CM4	NOAA	r1i1p1f1	Held et al., (2019)
GFDL-ESM4	NOAA	r1i1p1f1	Dunne et al. (2020)

GISS-E2-1-G-CC	NASA-GISS	r1i1p1f1	Kelley et al., (2020)
GISS-E2-1-G*	NASA-GISS	r1i1p1f2	Kelley et al., (2020)
HadGEM3-GC31-LL*	MOHC	r1i1p1f3	Kuhlbrodt et al. (2018)
HadGEM3-GC31-MM*	MOHC	r1i1p1f3	Andrews et al., (2020); Williams et al., (2018)
ICON-ESM-LR	MPI	r1i1p1f1	Jungclaus et al., (2022)
INM-CM4-8*	INM	r1i1p1f1	(Volodin et al. (2018)
INM-CM5-0*	INM	r1i1p1f1	Volodin & Gritsun (2018)
IPSL-CM6A-LR*	IPSL	r1i1p1f1	Boucher et al. (2020); Lurton et al. (2020)
IPSL-CM6A-LR-INCA	IPSL	r1i1p1f1	Boucher et al., (2020)
MIROC6*	JAMSTEC, NIES, AORI, U. of Tokyo	r1i1p1f1	Tatebe et al. (2019)
MPI-ESM-1-2-HAM	MPI	r1i1p1f1	Mauritsen et al. (2019)
MPI-ESM1-2-HR*	MPI	r1i1p1f1	Gutjahr et al. (2019); Müller et al. (2018)
MPI-ESM1-2-LR*	MPI	r1i1p1f1	Mauritsen et al. (2019)
MRI-ESM2-0*	MRI	r1i1p1f1	Yukimoto et al. (2019)
NorCPM1	NCC	r1i1p1f1	Bethke et al. (2021)
NorESM2-LM*	NCC	r1i1p1f1	Tjiputra et al. (2020)
NorESM2-MM*	NCC	r1i1p1f1	Tjiputra et al. (2020)
SAM0-UNICON	SNU	r1i1p1f1	Park et al. (2019)
UKESM1-0-LL*	MOHC	r1i1p1f2	Sellar et al. (2019)
UKESM1-1-LL	MOHC	r1i1p1f2	Sellar et al. (2019)

Table S1. List of the 49 CMIP6 models used in this study (i.e., the historical simulations that provide the overturning streamfunction). Models with a '*' superscript are used in our ssp585 experiment analysis.

	Observation-based estimates			
	GloRanV14 (2000-2021)	ECCOv4 (density space) (1992-2015)	Robust diagnostic simulation (Lee et al., 2019)	Inverse model estimate at 32°S (Lumpkin & Speer, 2007)
$AMOC_{max}$ (Sv)	18.9	18	25	18
AMOC_34.5°S (Sv)	15.6	14	16.9 (30°S)	12.4
$NADW\_wind_{total}$ (Sv)	7.6	14	-	11
$NADW\_IP_{diffu}$ (Sv)	8.1	0	~6.5	1.4
AMOC weakening based on emergent constraint (Sv) (2080-2100, ssp126 forcing)	6.0 (32%) (36% relative to RAPID AMOC)	3.0 (17%) (18% relative to RAPID AMOC)	5.4 (22%) (32% relative to RAPID AMOC)	3.5 (19%) (21% relative to RAPID AMOC)
AMOC weakening based on emergent constraint (Sv) (2080-2100, ssp585 forcing)	11.6 (61%) (67% relative to RAPID AMOC)	5.2 (29%) (31% relative to RAPID AMOC)	10.3 (41%) (61% relative to RAPID AMOC)	6.3 (35%) (37% relative to RAPID AMOC)

Table S2. Observation-based estimates of the AMOC strength, the overturning pathways and the AMOC weakening by 2080-2100 based on the CMIP6 Indo-Pacific diffusive pathway emergent constraint relationship under ssp126 and ssp585 forcing. The % weakening is shown relative to $AMOC_{max}$ in the observation-based estimate and relative to the time-mean RAPID/MOCHA (Rapid Climate Change-Meridional Overturning Circulation and Heatflux Array) AMOC estimate at 26.5°N of 16.9 Sv, averaged from April 2004 to September 2018 (Moat et al., 2022).

No	MOC Pathway	Abbreviation	Definition
(1)	Atlantic diffusive pathway	"NADW_At$_{diffu}$"	NADW pathway that upwells diffusively (or via eddy-induced circulations) in the Atlantic basin and returns to the North Atlantic at shallower depths without entering the Southern Ocean (SO).
(2)	Total Southern Ocean wind pathway	"NADW_wind$_{total}$" (4) + (5)	Total volume of the AMOC upwelled by the SO upper wind-driven cell that is approximately equal to the strength of the SO upper cell at 34.5°S.
(3)	Total Indo-Pacific pathway	"NADW_IP$_{total}$" (5) + (6)	NADW pathway that flows into the Indo-Pacific basin via the SO, upwells diffusively and returns at shallower depths to the Atlantic basin.
(4)	Atlantic wind pathway	"NADW_At$_{wind}$"	NADW pathway that flows out of the Atlantic basin into the global-integrated SO wind-driven upper cell (i.e., flows into the SO above "Z_(SO_upper_cell)" in Figure 1) where it upwells and returns directly to the Atlantic basin at shallower depths.
(5)	Indo-Pacific wind pathway	"NADW_IP$_{wind}$"	Component of the Indo-Pacific pathway that upwells diffusively in the Indo-Pacific basin and is then upwelled further by the SO wind-driven upper cell, before returning to the Atlantic basin.
(6)	Indo-Pacific diffusive pathway	"NADW_IP$_{diffu}$"	Component of the Indo-Pacific pathway that upwells diffusively in the Indo-Pacific basin and then returns directly to the Atlantic basin via zonal flows in the SO (i.e., it is not upwelled by the SO upper cell).
(7)	Lower Indo-Pacific pathway	"NADW_IP$_{lower}$"	NADW pathway that flows out of the Atlantic basin into the global-integrated SO lower cell (i.e., below "Z_(SO_upper_cell)" in Figure 1), and then into the Indo-Pacific basin.
(8)	Upper Indo-Pacific pathway	"NADW_IP$_{upper}$"	NADW pathway that flows southward into the global-integrated SO upper cell (i.e., above "Z_(SO_upper_cell)"), and then into the Indo-Pacific basin.

Table S3. Overturning pathway definitions

Name	Definition
AMOC$_{max}$	Maximum strength of the AMOC in the North Atlantic
Z_AMOC	Depth of AMOC in the South Atlantic at 34.5°S
Z_(SO upper cell)	Depth of globally-integrated Southern Ocean (SO) upper cell at 34.5°S
Cell overlap	Depth of the overlap between the AMOC and the globally-integrated Southern Ocean lower cell at 34.5°S i.e., "Z_AMOC" – "Z_(SO upper cell)"

Table S4. Definitions of key terms and abbreviations

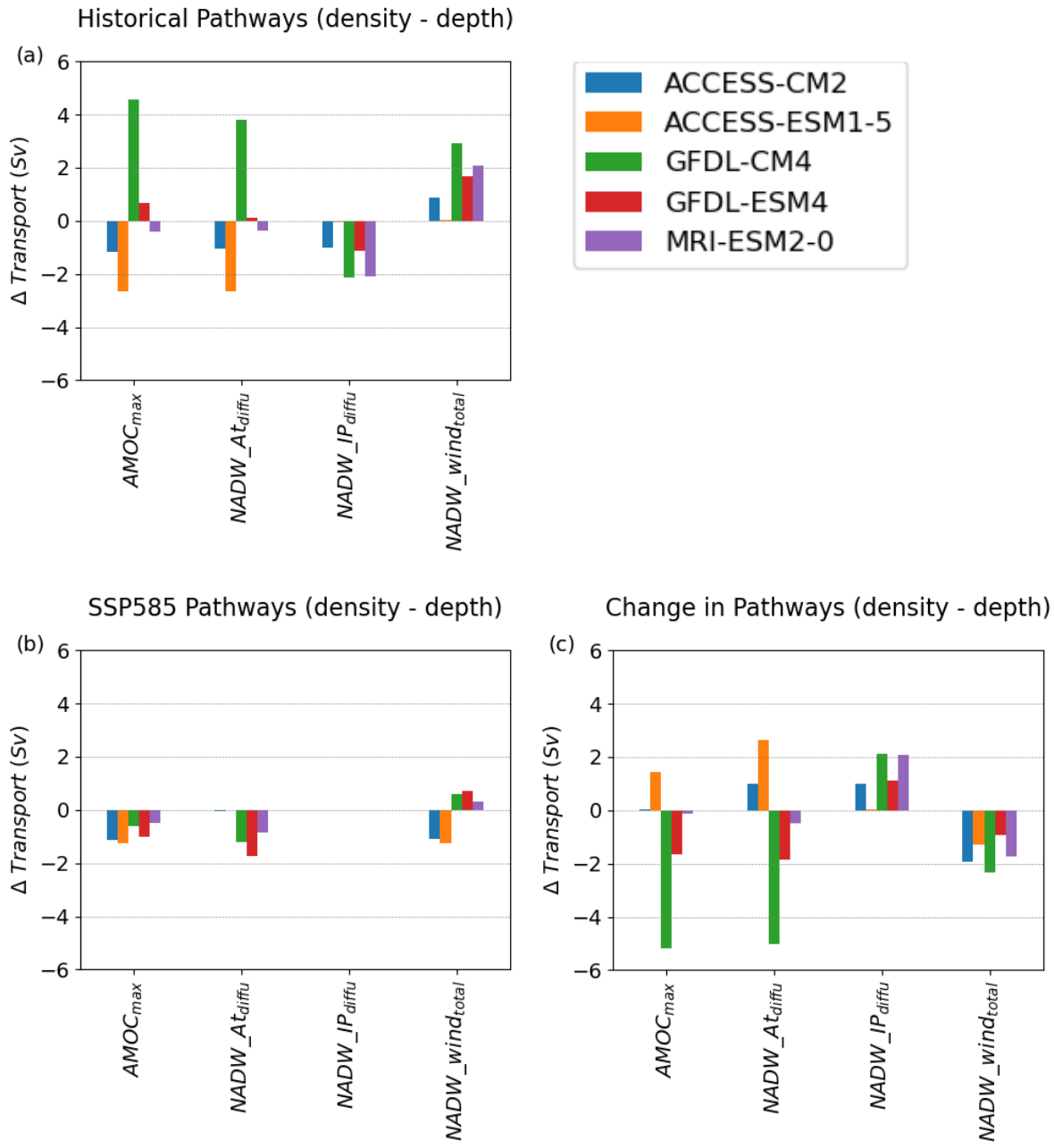

Figure S1. Difference between the AMOC strength and overturning pathways calculated in depth and density space in (a) the historical simulation (185-2014), (b) 2080-2100 of the ssp585 experiment and (c) the change between the historical simulation and 2080-2100 of ssp585.

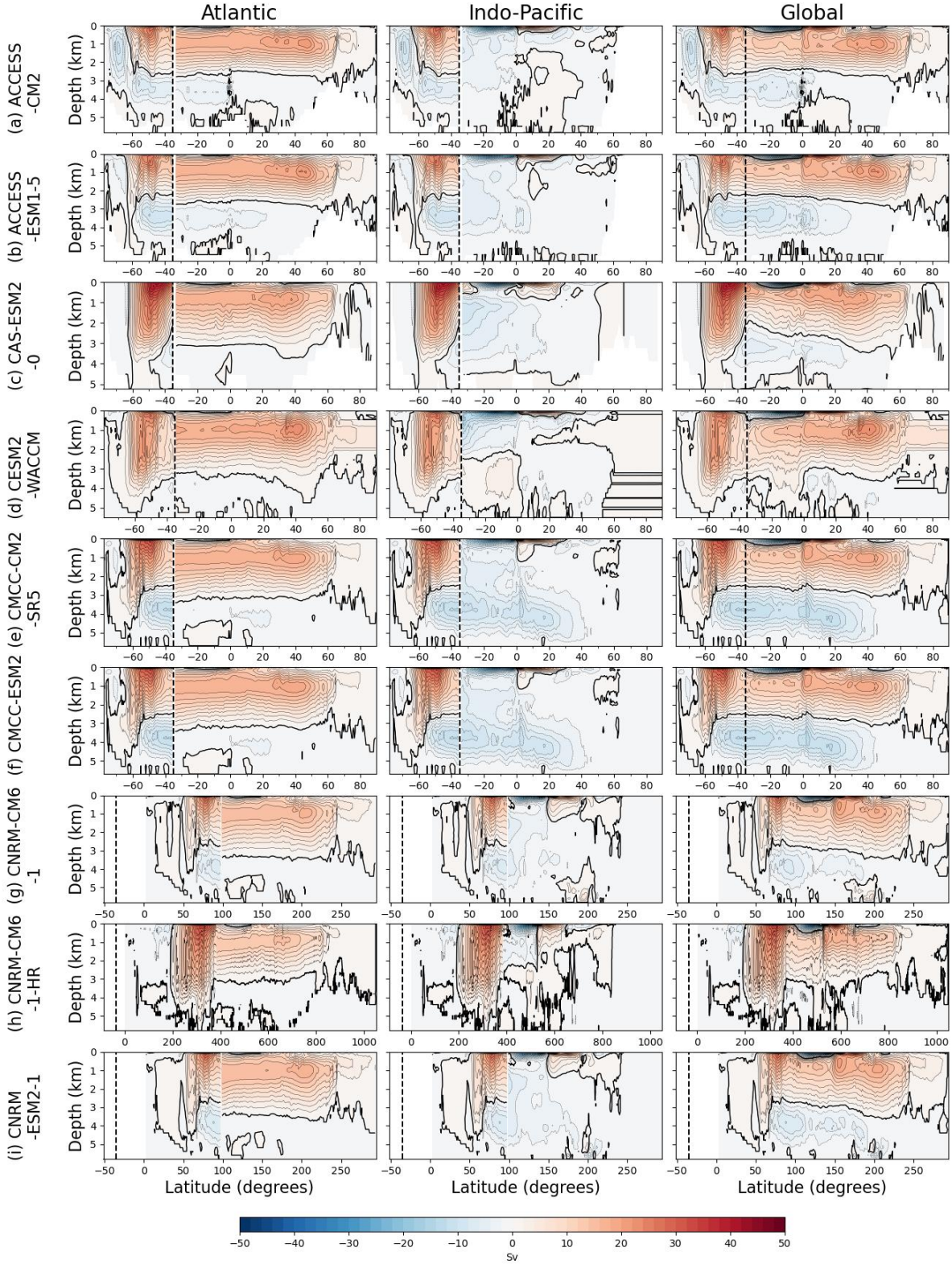
Atlantic
Indo-Pacific
Global
(a) ACCESS -CM2
(b) ACCESS -ESM1-5
(c) CAS-ESM2 -0
(d) CESM2 -WACCM
(e) CMCC-CM2 -SR5
(f) CMCC-ESM2
(g) CNRM-CM6 -1
(h) CNRM-CM6 -1-HR
(i) CNRM -ESM2-1
Depth (km)
Latitude (degrees)
Sv

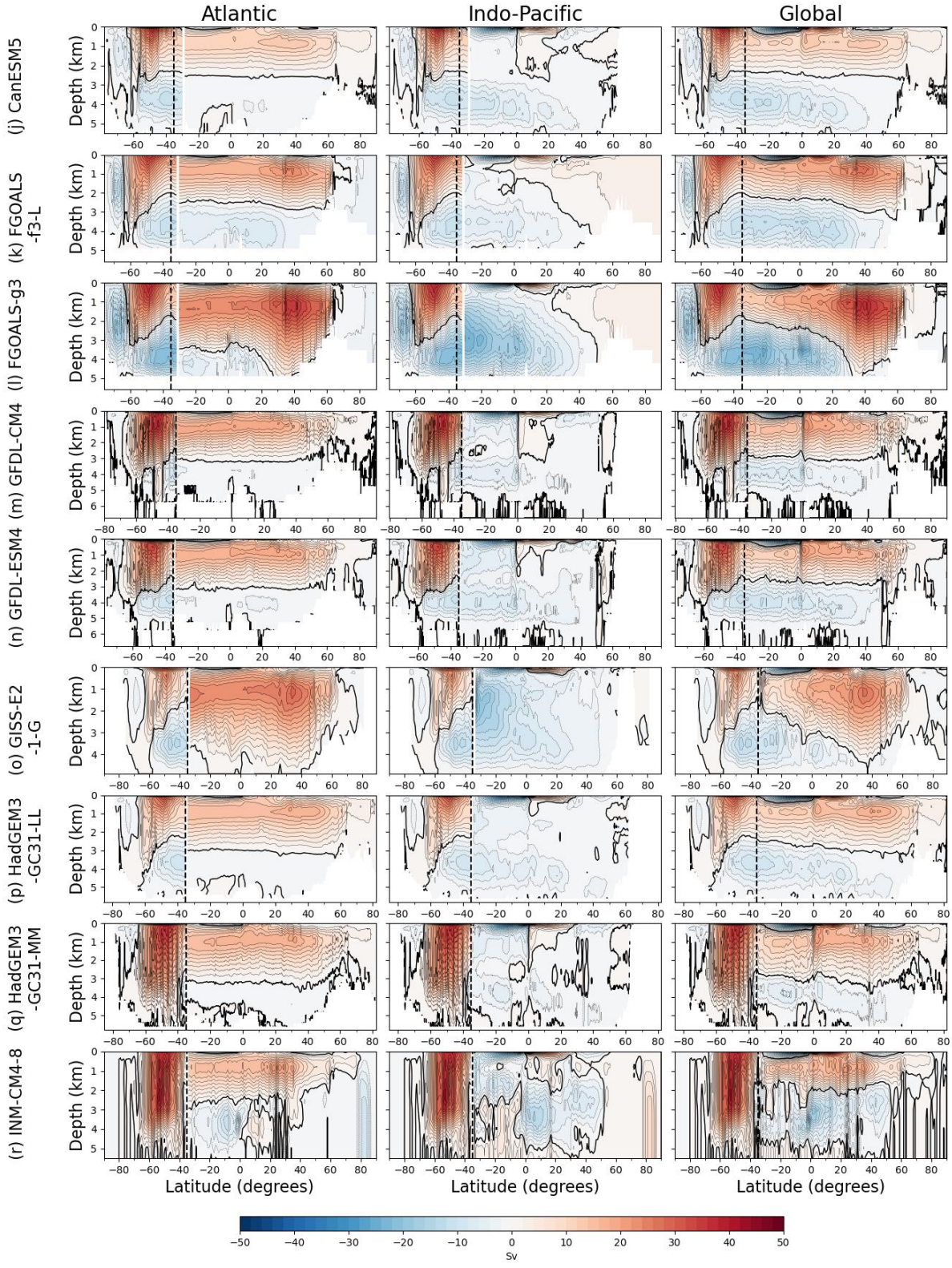
Atlantic
Indo-Pacific
Global
(j) CanESM5
(k) FGOALS -f3-L
(l) FGOALS-g3
(m) GFDL-CM4
(n) GFDL-ESM4
(o) GISS-E2 -1-G
(p) HadGEM3 -GC31-LL
(q) HadGEM3 -GC31-MM
(r) INM-CM4-8
Depth (km)
Latitude (degrees)
Sv

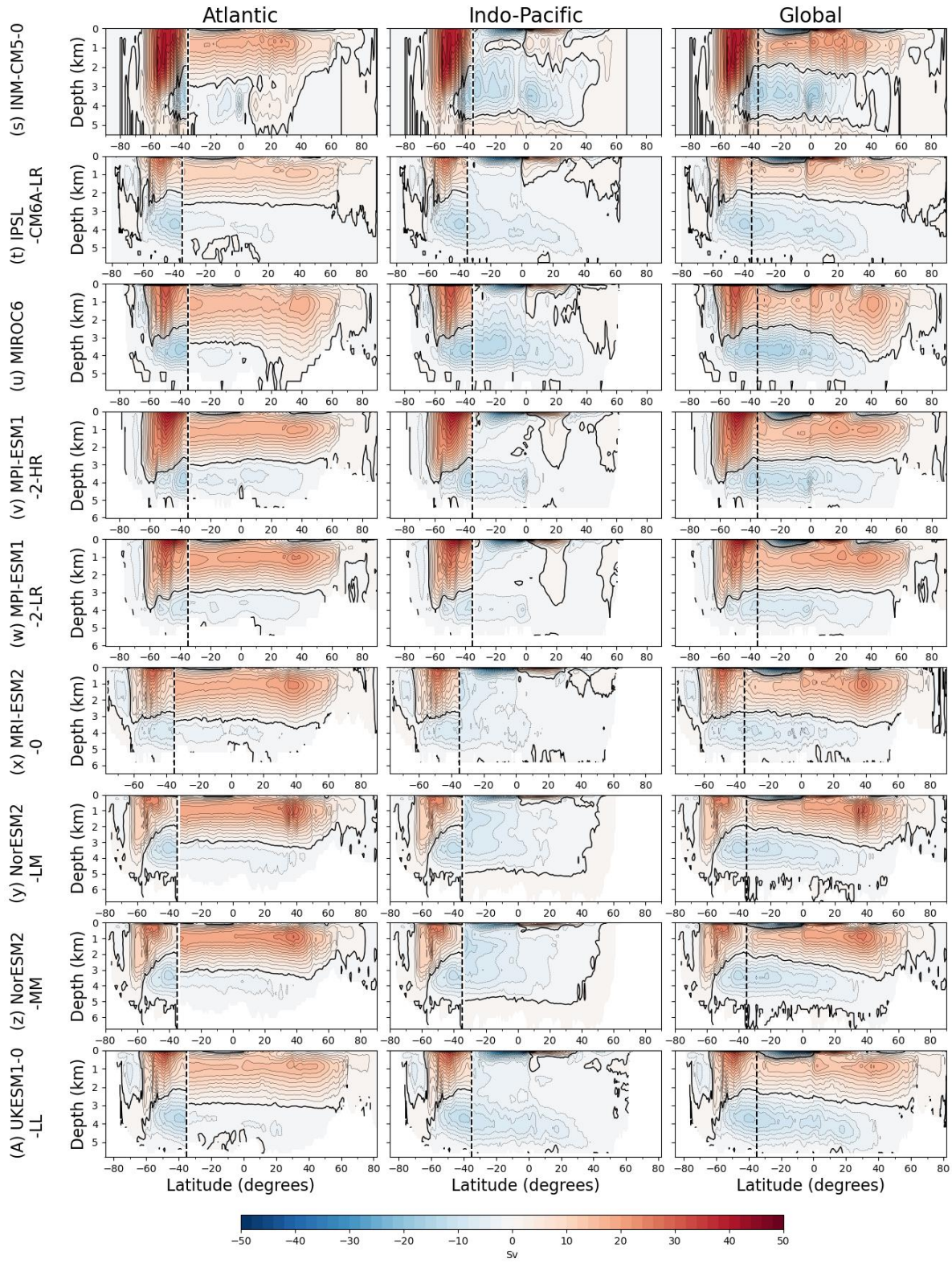

Figure S2. Overturning streamfunction (Sverdrups (Sv); 2 Sv contour interval) in depth space averaged over the 1850-2014 historical simulation in each model that has a ssp585 experiment. The zero-streamline contour is defined by the thick black line.

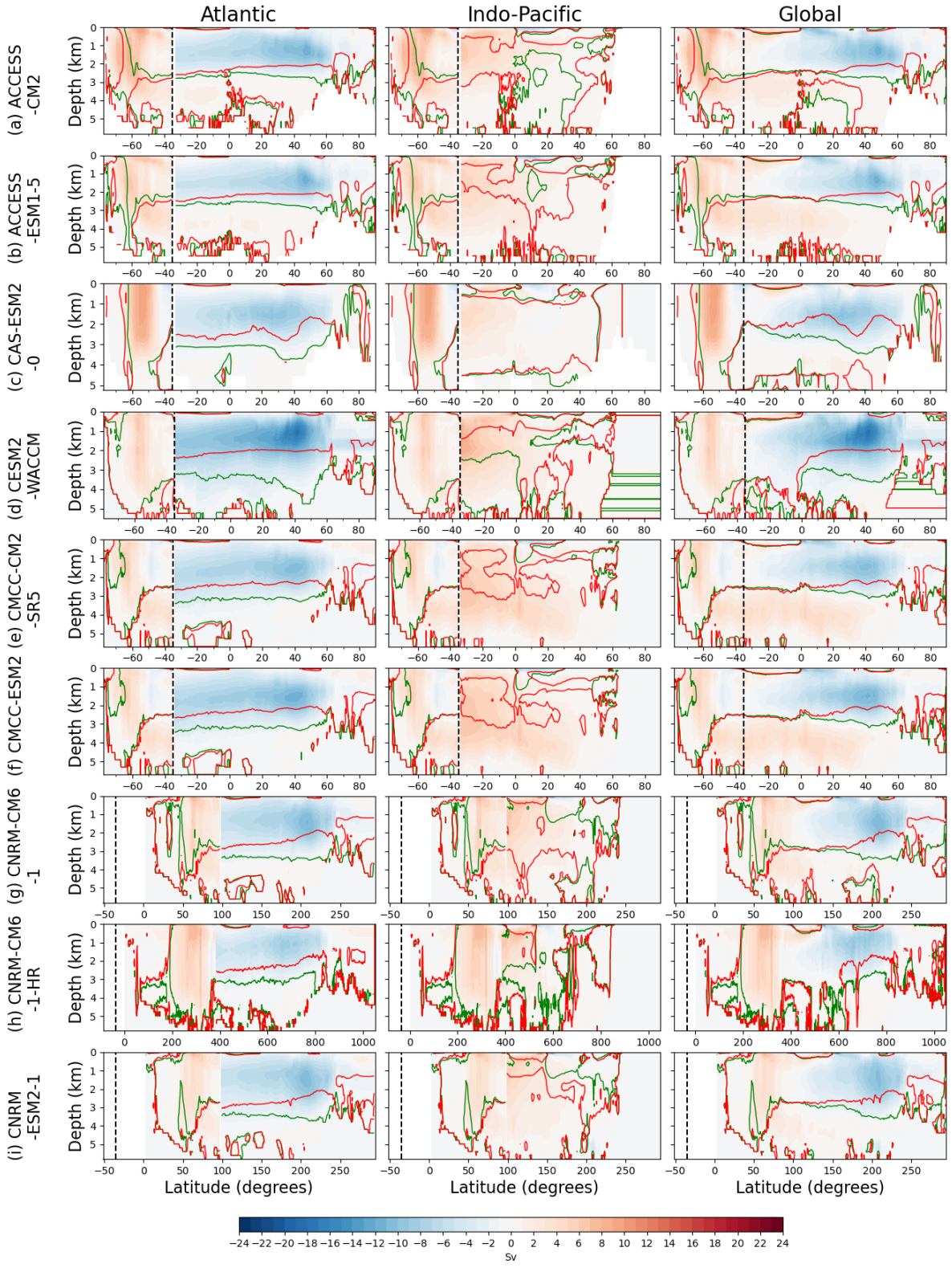
Atlantic
Indo-Pacific
Global
(a) ACCESS -CM2
(b) ACCESS -ESM1-5
(c) CAS-ESM2 -0
(d) CESM2 -WACCM
(e) CMCC-CM2 -SR5
(f) CMCC-ESM2
(g) CNRM-CM6 -1
(h) CNRM-CM6 -1-HR
(i) CNRM -ESM2-1
Depth (km)
Latitude (degrees)
Sv

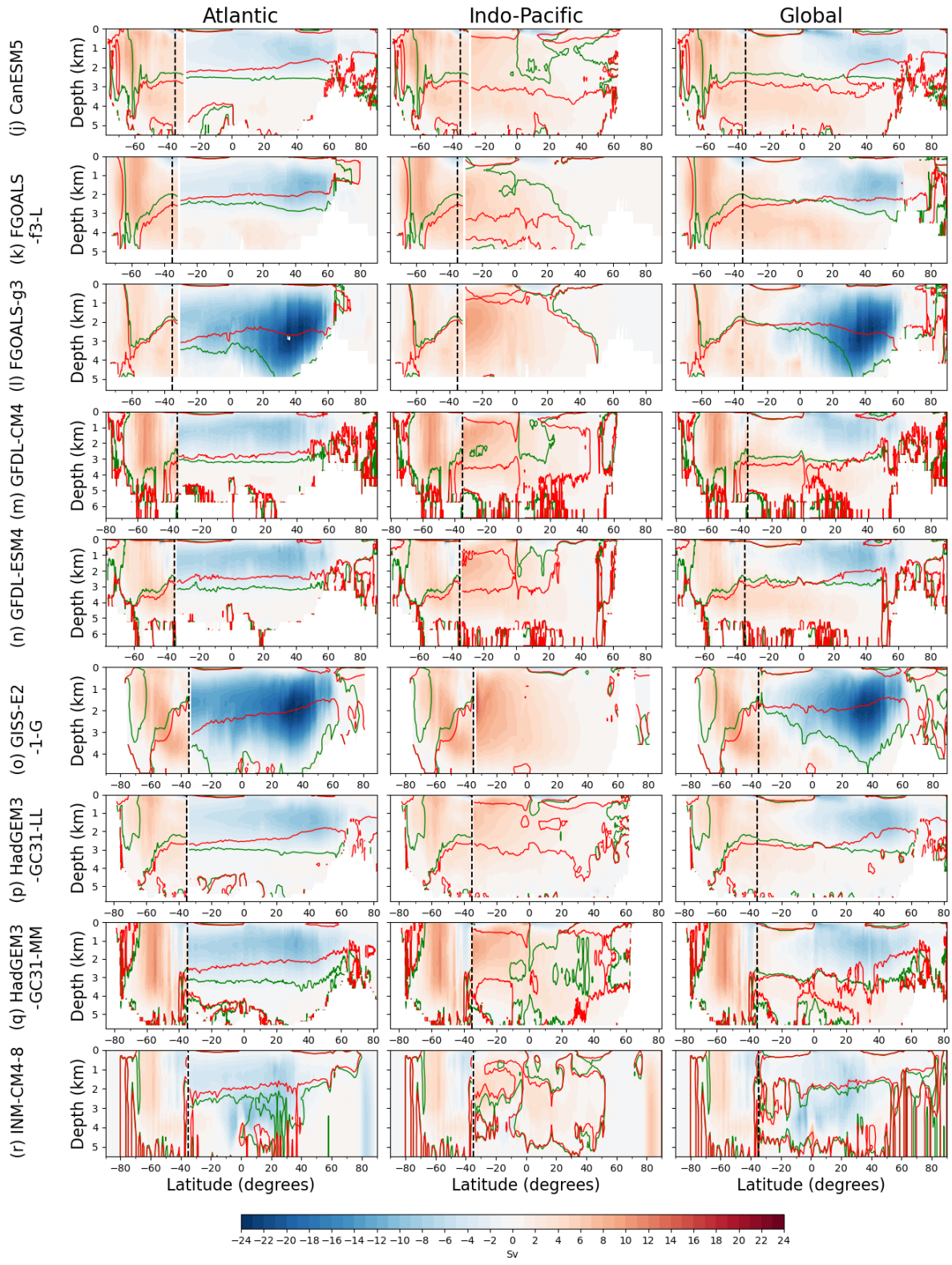
Atlantic
Indo-Pacific
Global
(j) CanESM5
(k) FGOALS -f3-L
(l) FGOALS-g3
(m) GFDL-CM4
(n) GFDL-ESM4
(o) GISS-E2 -1-G
(p) HadGEM3 -GC31-LL
(q) HadGEM3 -GC31-MM
(r) INM-CM4-8
Depth (km)
Latitude (degrees)
Sv

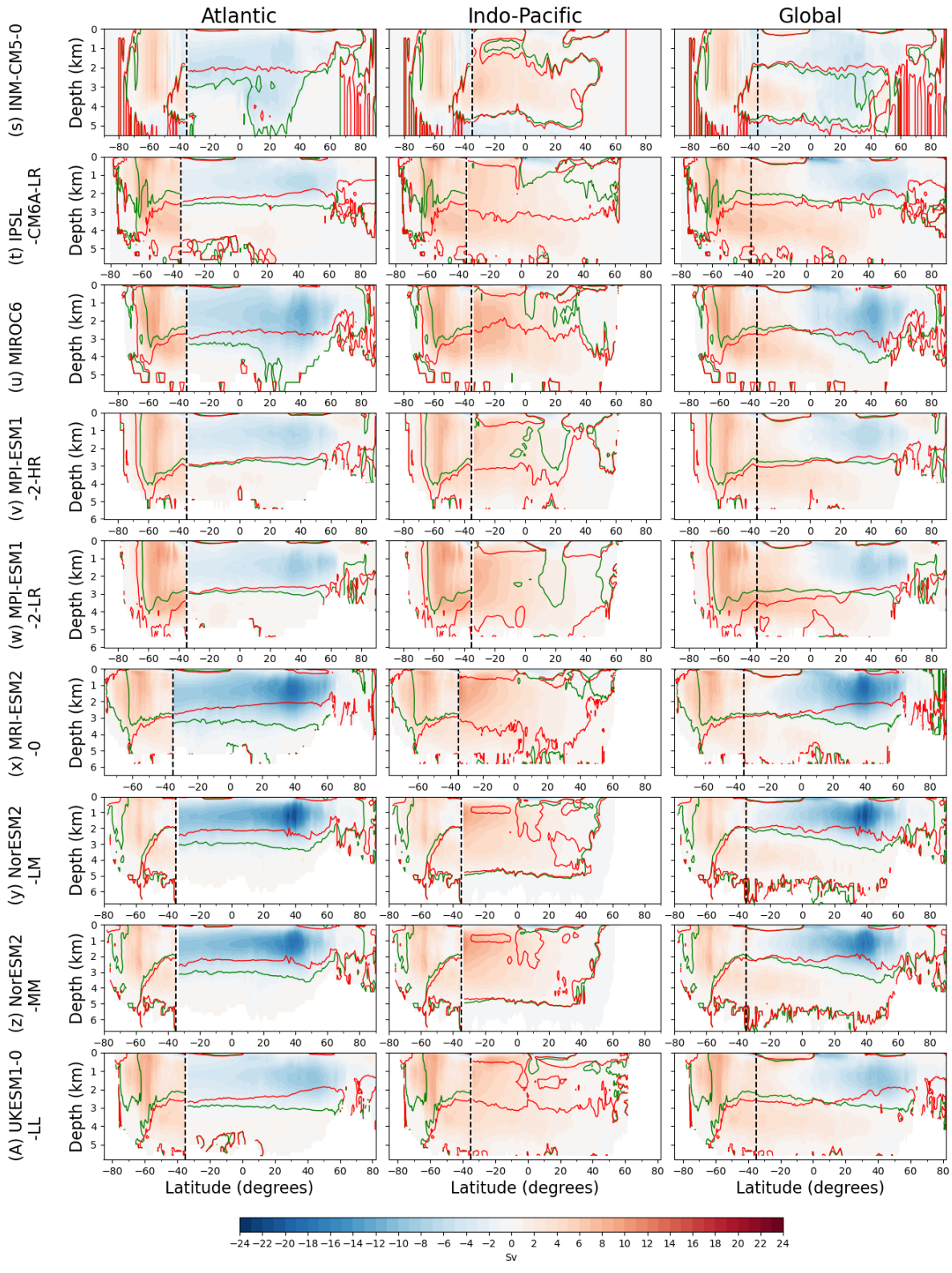

Figure S3. Changes in the overturning streamfunction (Sverdrups (Sv); 1 Sv contour interval) in depth space for the Atlantic, Indo-Pacific and global-average, calculated as the difference between the ssp585 experiment averaged over 2080-2100 and the historical experiment averaged over 1850-2014. The zero-streamline contour averaged over the historical simulation (green line) and from the 2080-2100 period of ssp585 (red line) are overlayed, so the location of the overturning cells and thus changes in the "cell overlap" can be inferred.

Equations used to separate the MOC pathways

We now define the equations linking the MOC pathways:

$$AMOC_{max} = NADW\_At_{diffu} + AMOC\,|_{\phi = 34.5°S} \quad \text{(eq. S1)}$$

$$NADW\_At_{diffu} = AMOC_{max} - AMOC\,|_{\phi = 34.5°S} \quad \text{(eq. S2)}$$

$$AMOC\,|_{\phi = 34.5°S} = NADW\_At_{wind} + NADW\_IP_{total}$$

$$= NADW\_wind_{total} + NADW\_IP_{diffu} \quad \text{(eq. S3)}$$

$$NADW\_IP_{wind} = NADW\_wind_{total} - NADW\_At_{wind} \quad \text{(eq. S4)}$$

$$NADW\_IP_{diffu} = NADW\_IP_{total} - NADW\_IP_{wind} \quad \text{(eq. S5)}$$

Modifications to the method of Baker et al. (2020,2021) *(BWV)*

We make several modifications to the *BWV* method to calculate the overturning pathways since we must account for overturning structures that were not present in the idealised model simulations of *BWV*. For example, a few of the CMIP6 models (e.g., CasESM) have localised clockwise meridional overturning cells at the southern boundary of the Indo-Pacific basin (see Figure S1). These cells export water southwards out of the Indo-Pacific basin, where, depending on their depth, they may upwell via the Southern Ocean (SO) upper cell. The magnitude of the Atlantic wind pathway or the Indo-Pacific wind pathway (and thus the total SO wind pathway) is therefore lower than that calculated using the original method due to upwelling of the NADW pathways by the SO upper cell decreasing (i.e., a reduced "total SO wind pathway").

In some models, the upper overturning streamfunction in the South Atlantic is not entirely connected to the NADW formation and subduction region in the North Atlantic. Instead, there is a "localised" circulation in both the North and South Atlantic, with no connection between these cells. Thus, when calculating the pathways of NADW, we reduce the pathway into the SO if a "localised" circulation is present in the South Atlantic. We determine the magnitude of this modified pathway by setting the pathway of NADW into the SO equal to the minimum AMOC strength located between 34.5°S and the latitude of the AMOC maximum in the North Atlantic. The remaining pathways are calculated as described previously, but using the modified pathway into the SO, $AMOC\,|_{\phi = 34.5°S}$. The Atlantic diffusive pathway calculated using the original method is increased by a magnitude equal to

the reduction in the pathway into the SO. Further modifications to the pathways are required if the "localised" South Atlantic MOC is upwelled by the SO upper cell as opposed to upwelling in the Indo-Pacific basin. We must then reduce the total SO wind pathway and increase the Indo-Pacific diffusive pathway by an equal magnitude. The proportion of the "localised" South Atlantic MOC that is upwelled in the Indo-Pacific basin is calculated from the change in the Indo-Pacific streamfunction at 34.5°S over the depth (or density range) of the "localised" cell. We note that while important, the differences when using this modified method do not change the qualitative results with similar correlations between the pathways and AMOC weakening.

Differences between depth and density space

We compare the overturning pathways calculated in depth and density space in five models, averaged over the historical simulation and over 2080-2100 in ssp585. Differences in the total SO wind and Indo-Pacific diffusive pathways are small relative to their absolute magnitudes (Figure S3a,b). In contrast, the Atlantic diffusive pathway has larger differences between these coordinate spaces in some models (Figure S3a,b), resulting in differences in AMOC strength and AMOC weakening (Figure S3c). Thus, the quantitative dependence of the AMOC weakening on both the historical AMOC strength and historical overturning pathways would change in density space. However, we expect our qualitative findings to be applicable in density space because the Indo-Pacific diffusive pathway is not significantly affected. The historical magnitude of this pathway is only slightly smaller in density space in most models. Thus, while the correlation between the Indo-Pacific diffusive pathway and AMOC weakening may differ in density space, it is likely be similar.

References

Andrews, M. B., Ridley, J. K., Wood, R. A., Andrews, T., Blockley, E. W., Booth, B., Burke, E., Dittus, A. J., Florek, P., Gray, L. J., Haddad, S., Hardiman, S. C., Hermanson, L., Hodson, D., Hogan, E., Jones, G. S., Knight, J. R., Kuhlbrodt, T., Misios, S., … Sutton, R. T. (2020). Historical Simulations With HadGEM3-GC3.1 for CMIP6. *Journal of Advances in Modeling Earth Systems*, *12*(6), e2019MS001995. https://doi.org/10.1029/2019MS001995

Bethke, I., Wang, Y., Counillon, F., Keenlyside, N., Kimmritz, M., Fransner, F., Samuelsen, A., Langehaug, H., Svendsen, L., Chiu, P. G., Passos, L., Bentsen, M., Guo, C., Gupta, A., Tjiputra, J., Kirkeväg, A., Olivié, Di., Seland, Ø., Solsvik Vägane, J., … Eldevik, T. (2021). NorCPM1 and its

contribution to CMIP6 DCPP. *Geoscientific Model Development*, *14*(11), 7073–7116. https://doi.org/10.5194/GMD-14-7073-2021

Bi, D., Dix, M., Marsland, S., O'farrell, S., Sullivan, A., Bodman, R., Law, R., Harman, I., Srbinovsky, J., Rashid, H. A., Dobrohotoff, P., Mackallah, C., Yan, H., Hirst, A., Savita, A., Boeira Dias, F., Woodhouse, M., Fiedler, R., & Heerdegen, A. (2020). Configuration and spin-up of ACCESS-CM2, the new generation Australian Community Climate and Earth System Simulator Coupled Model. *Journal of Southern Hemisphere Earth Systems Science*, *70*(1), 225–251. https://doi.org/10.1071/ES19040

Boucher, O., Servonnat, J., Albright, A. L., Aumont, O., Balkanski, Y., Bastrikov, V., Bekki, S., Bonnet, R., Bony, S., Bopp, L., Braconnot, P., Brockmann, P., Cadule, P., Caubel, A., Cheruy, F., Codron, F., Cozic, A., Cugnet, D., D'Andrea, F., … Vuichard, N. (2020). Presentation and Evaluation of the IPSL-CM6A-LR Climate Model. *Journal of Advances in Modeling Earth Systems*, *12*(7). https://doi.org/10.1029/2019MS002010

Cherchi, A., Fogli, P. G., Lovato, T., Peano, D., Iovino, D., Gualdi, S., Masina, S., Scoccimarro, E., Materia, S., Bellucci, A., & Navarra, A. (2019). Global Mean Climate and Main Patterns of Variability in the CMCC-CM2 Coupled Model. *Journal of Advances in Modeling Earth Systems*, *11*(1), 185–209. https://doi.org/10.1029/2018MS001369

Danabasoglu, G., Lamarque, J. F., Bacmeister, J., Bailey, D. A., DuVivier, A. K., Edwards, J., Emmons, L. K., Fasullo, J., Garcia, R., Gettelman, A., Hannay, C., Holland, M. M., Large, W. G., Lauritzen, P. H., Lawrence, D. M., Lenaerts, J. T. M., Lindsay, K., Lipscomb, W. H., Mills, M. J., … Strand, W. G. (2020). The Community Earth System Model Version 2 (CESM2). *Journal of Advances in Modeling Earth Systems*, *12*(2), e2019MS001916. https://doi.org/10.1029/2019MS001916

Dunne, J. P., Horowitz, L. W., Adcroft, A. J., Ginoux, P., Held, I. M., John, J. G., Krasting, J. P., Malyshev, S., Naik, V., Paulot, F., Shevliakova, E., Stock, C. A., Zadeh, N., Balaji, V., Blanton, C., Dunne, K. A., Dupuis, C., Durachta, J., Dussin, R., … Zhao, M. (2020). The GFDL Earth System Model Version 4.1 (GFDL-ESM 4.1): Overall Coupled Model Description and Simulation Characteristics. *Journal of Advances in Modeling Earth Systems*, *12*(11), e2019MS002015. https://doi.org/10.1029/2019MS002015

Golaz, J. C., Caldwell, P. M., van Roekel, L. P., Petersen, M. R., Tang, Q., Wolfe, J. D., Abeshu, G., Anantharaj, V., Asay-Davis, X. S., Bader, D. C., Baldwin, S. A., Bisht, G., Bogenschutz, P. A., Branstetter, M., Brunke, M. A., Brus, S. R., Burrows, S. M., Cameron-Smith, P. J., Donahue, A. S., … Zhu, Q. (2019). The DOE E3SM Coupled Model Version 1: Overview and Evaluation at Standard Resolution. *Journal of Advances in Modeling Earth Systems*, *11*(7), 2089–2129. https://doi.org/10.1029/2018MS001603

Gutjahr, O., Putrasahan, D., Lohmann, K., Jungclaus, J. H., von Storch, J. S., Brüggemann, N., Haak, H., & Stössel, A. (2019). Max Planck Institute Earth System Model (MPI-ESM1.2) for the High-Resolution Model Intercomparison Project (HighResMIP). *Geoscientific Model Development*, *12*(7), 3241–3281. https://doi.org/10.5194/GMD-12-3241-2019

He, B., Yu, Y., Bao, Q., Lin, P., Liu, H., Li, J., Wang, L., Liu, Y., Wu, G., Chen, K., Guo, Y., Zhao, S., Zhang, X., Song, M., Xie, J., Bian, H. E., Yongqiang, Y. U., Qing, B., Pengfei, L., … Jinbo, X. (2020). CAS FGOALS-f3-L model dataset descriptions for CMIP6 DECK experiments. *New Pub: KeAi*, 582–588. https://doi.org/10.1080/16742834.2020.1778419

Held, I. M., Guo, H., Adcroft, A., Dunne, J. P., Horowitz, L. W., Krasting, J., Shevliakova, E., Winton, M., Zhao, M., Bushuk, M., Wittenberg, A. T., Wyman, B., Xiang, B., Zhang, R., Anderson, W., Balaji, V., Donner, L., Dunne, K., Durachta, J., … Zadeh, N. (2019). Structure and Performance of GFDL's CM4.0 Climate Model. *Journal of Advances in Modeling Earth Systems*, *11*(11), 3691–3727. https://doi.org/10.1029/2019MS001829

Jungclaus, J. H., Lorenz, S. J., Schmidt, H., Brovkin, V., Brüggemann, N., Chegini, F., Crüger, T., De-Vrese, P., Gayler, V., Giorgetta, M. A., Gutjahr, O., Haak, H., Hagemann, S., Hanke, M., Ilyina, T., Korn, P., Kröger, J., Linardakis, L., Mehlmann, C., … Claussen, M. (2022). The ICON Earth System Model Version 1.0. *Journal of Advances in Modeling Earth Systems*, *14*(4), e2021MS002813. https://doi.org/10.1029/2021MS002813

Kelley, M., Schmidt, G. A., Nazarenko, L. S., Bauer, S. E., Ruedy, R., Russell, G. L., Ackerman, A. S., Aleinov, I., Bauer, M., Bleck, R., Canuto, V., Cesana, G., Cheng, Y., Clune, T. L., Cook, B. I., Cruz, C. A., del Genio, A. D., Elsaesser, G. S., Faluvegi, G., … Yao, M. S. (2020). GISS-E2.1: Configurations and Climatology. *Journal of Advances in Modeling Earth Systems*, *12*(8), e2019MS002025. https://doi.org/10.1029/2019MS002025

Kuhlbrodt, T., Jones, C. G., Sellar, A., Storkey, D., Blockley, E., Stringer, M., Hill, R., Graham, T., Ridley, J., Blaker, A., Calvert, D., Copsey, D., Ellis, R., Hewitt, H., Hyder, P., Ineson, S., Mulcahy, J., Siahaan, A., & Walton, J. (2018). The Low-Resolution Version of HadGEM3 GC3.1: Development and Evaluation for Global Climate. *Journal of Advances in Modeling Earth Systems*, *10*(11), 2865–2888. https://doi.org/10.1029/2018MS001370

Lee, S. K., Lumpkin, R., Baringer, M. O., Meinen, C. S., Goes, M., Dong, S., Lopez, H., & Yeager, S. G. (2019). Global Meridional Overturning Circulation Inferred From a Data-Constrained Ocean & Sea-Ice Model. *Geophysical Research Letters*, *46*(3), 1521–1530. https://doi.org/10.1029/2018GL080940

Li, L., Yu, Y., Tang, Y., Lin, P., Xie, J., Song, M., Dong, L., Zhou, T., Liu, L., Wang, L., Pu, Y., Chen, X., Chen, L., Xie, Z., Liu, H., Zhang, L., Huang, X., Feng, T., Zheng, W., … Wei, J. (2020). The Flexible Global Ocean-Atmosphere-Land System Model Grid-Point Version 3 (FGOALS-g3): Description and Evaluation. *Journal of Advances in Modeling Earth Systems*, *12*(9), e2019MS002012. https://doi.org/10.1029/2019MS002012

Lin, Y., Huang, X., Liang, Y., Qin, Y., Xu, S., Huang, W., Xu, F., Liu, L., Wang, Y., Peng, Y., Wang, L., Xue, W., Fu, H., Zhang, G. J., Wang, B., Li, R., Zhang, C., Lu, H., Yang, K., … Gong, P. (2020). Community Integrated Earth System Model (CIESM): Description and Evaluation. *Journal of Advances in Modeling Earth Systems*, *12*(8), e2019MS002036. https://doi.org/10.1029/2019MS002036

Lovato, T., Peano, D., Butenschön, M., Materia, S., Iovino, D., Scoccimarro, E., Fogli, P. G., Cherchi, A., Bellucci, A., Gualdi, S., Masina, S., & Navarra, A. (2022). CMIP6 Simulations With the CMCC Earth System Model (CMCC-ESM2). *Journal of Advances in Modeling Earth Systems*, *14*(3), e2021MS002814. https://doi.org/10.1029/2021MS002814

Lumpkin, R., & Speer, K. (2007). Global Ocean Meridional Overturning. *Journal of Physical Oceanography*, *37*(10), 2550–2562. https://doi.org/10.1175/JPO3130.1

Lurton, T., Balkanski, Y., Bastrikov, V., Bekki, S., Bopp, L., Braconnot, P., Brockmann, P., Cadule, P., Contoux, C., Cozic, A., Cugnet, D., Dufresne, J. L., Éthé, C., Foujols, M. A., Ghattas, J., Hauglustaine, D., Hu, R. M., Kageyama, M., Khodri, M., … Boucher, O. (2020). Implementation

of the CMIP6 Forcing Data in the IPSL-CM6A-LR Model. *Journal of Advances in Modeling Earth Systems*, *12*(4), e2019MS001940. https://doi.org/10.1029/2019MS001940

Mauritsen, T., Bader, J., Becker, T., Behrens, J., Bittner, M., Brokopf, R., Brovkin, V., Claussen, M., Crueger, T., Esch, M., Fast, I., Fiedler, S., Fläschner, D., Gayler, V., Giorgetta, M., Goll, D. S., Haak, H., Hagemann, S., Hedemann, C., … Roeckner, E. (2019). Developments in the MPI-M Earth System Model version 1.2 (MPI-ESM1.2) and Its Response to Increasing CO2. *Journal of Advances in Modeling Earth Systems*, *11*(4), 998–1038. https://doi.org/10.1029/2018MS001400

Müller, W. A., Jungclaus, J. H., Mauritsen, T., Baehr, J., Bittner, M., Budich, R., Bunzel, F., Esch, M., Ghosh, R., Haak, H., Ilyina, T., Kleine, T., Kornblueh, L., Li, H., Modali, K., Notz, D., Pohlmann, H., Roeckner, E., Stemmler, I., … Marotzke, J. (2018). A Higher-resolution Version of the Max Planck Institute Earth System Model (MPI-ESM1.2-HR). *Journal of Advances in Modeling Earth Systems*, *10*(7), 1383–1413. https://doi.org/10.1029/2017MS001217

Park, S., Shin, J., Kim, S., Oh, E., & Kim, Y. (2019). Global Climate Simulated by the Seoul National University Atmosphere Model Version 0 with a Unified Convection Scheme (SAM0-UNICON). *Journal of Climate*, *32*(10), 2917–2949. https://doi.org/10.1175/JCLI-D-18-0796.1

Séférian, R., Nabat, P., Michou, M., Saint-Martin, D., Voldoire, A., Colin, J., Decharme, B., Delire, C., Berthet, S., Chevallier, M., Sénési, S., Franchisteguy, L., Vial, J., Mallet, M., Joetzjer, E., Geoffroy, O., Guérémy, J. F., Moine, M. P., Msadek, R., … Madec, G. (2019). Evaluation of CNRM Earth System Model, CNRM-ESM2-1: Role of Earth System Processes in Present-Day and Future Climate. *Journal of Advances in Modeling Earth Systems*, *11*(12), 4182–4227. https://doi.org/10.1029/2019MS001791

Sellar, A. A., Jones, C. G., Mulcahy, J. P., Tang, Y., Yool, A., Wiltshire, A., O'Connor, F. M., Stringer, M., Hill, R., Palmieri, J., Woodward, S., de Mora, L., Kuhlbrodt, T., Rumbold, S. T., Kelley, D. I., Ellis, R., Johnson, C. E., Walton, J., Abraham, N. L., … Zerroukat, M. (2019). UKESM1: Description and Evaluation of the U.K. Earth System Model. *Journal of Advances in Modeling Earth Systems*, *11*(12), 4513–4558. https://doi.org/10.1029/2019MS001739

Swart, N. C., Cole, J. N. S., Kharin, V. v., Lazare, M., Scinocca, J. F., Gillett, N. P., Anstey, J., Arora, V., Christian, J. R., Hanna, S., Jiao, Y., Lee, W. G., Majaess, F., Saenko, O. A., Seiler, C., Seinen, C., Shao, A., Sigmond, M., Solheim, L., … Winter, B. (2019). The Canadian Earth System Model version 5 (CanESM5.0.3). *Geoscientific Model Development*, *12*(11), 4823–4873. https://doi.org/10.5194/GMD-12-4823-2019

Tatebe, H., Ogura, T., Nitta, T., Komuro, Y., Ogochi, K., Takemura, T., Sudo, K., Sekiguchi, M., Abe, M., Saito, F., Chikira, M., Watanabe, S., Mori, M., Hirota, N., Kawatani, Y., Mochizuki, T., Yoshimura, K., Takata, K., O'Ishi, R., … Kimoto, M. (2019). Description and basic evaluation of simulated mean state, internal variability, and climate sensitivity in MIROC6. *Geoscientific Model Development*, *12*(7), 2727–2765. https://doi.org/10.5194/GMD-12-2727-2019

Tjiputra, J. F., Schwinger, J., Bentsen, M., L. Morée, A., Gao, S., Bethke, I., Heinze, C., Goris, N., Gupta, A., He, Y. C., Olivié, D., Seland, O., & Schulz, M. (2020). Ocean biogeochemistry in the Norwegian Earth System Model version 2 (NorESM2). *Geoscientific Model Development*, *13*(5), 2393–2431. https://doi.org/10.5194/GMD-13-2393-2020

Voldoire, A., Saint-Martin, D., Sénési, S., Decharme, B., Alias, A., Chevallier, M., Colin, J., Guérémy, J. F., Michou, M., Moine, M. P., Nabat, P., Roehrig, R., Salas y Mélia, D., Séférian, R., Valcke, S.,

Beau, I., Belamari, S., Berthet, S., Cassou, C., … Waldman, R. (2019). Evaluation of CMIP6 DECK Experiments With CNRM-CM6-1. *Journal of Advances in Modeling Earth Systems*, *11*(7), 2177–2213. https://doi.org/10.1029/2019MS001683

Volodin, E., & Gritsun, A. (2018). Simulation of observed climate changes in 1850-2014 with climate model INM-CM5. *Earth Syst. Dynam*, *9*, 1235–1242. https://doi.org/10.5194/esd-9-1235-2018

Volodin, E. M., Mortikov, E. v., Kostrykin, S. v., Galin, V. Y., Lykossov, V. N., Gritsun, A. S., Diansky, N. A., Gusev, A. v., Iakovlev, N. G., Shestakova, A. A., & Emelina, S. v. (2018). Simulation of the modern climate using the INM-CM48 climate model. *Russian Journal of Numerical Analysis and Mathematical Modelling*, *33*(6), 367–374. https://doi.org/10.1515/RNAM-2018-0032/MACHINEREADABLECITATION/RIS

Williams, K. D., Copsey, D., Blockley, E. W., Bodas-Salcedo, A., Calvert, D., Comer, R., Davis, P., Graham, T., Hewitt, H. T., Hill, R., Hyder, P., Ineson, S., Johns, T. C., Keen, A. B., Lee, R. W., Megann, A., Milton, S. F., Rae, J. G. L., Roberts, M. J., … Xavier, P. K. (2018). The Met Office Global Coupled Model 3.0 and 3.1 (GC3.0 and GC3.1) Configurations. *Journal of Advances in Modeling Earth Systems*, *10*(2), 357–380. https://doi.org/10.1002/2017MS001115

Wyser, K., van Noije, T., Yang, S., von Hardenberg, J., O'Donnell, D., & Döscher, R. (2020). On the increased climate sensitivity in the EC-Earth model from CMIP5 to CMIP6. *Geoscientific Model Development*, *13*(8), 3465–3474. https://doi.org/10.5194/GMD-13-3465-2020

Yukimoto, S., Kawai, H., Koshiro, T., Oshima, N., Yoshida, K., Urakawa, S., Tsujino, H., Deushi, M., Tanaka, T., Hosaka, M., Yabu, S., Yoshimura, H., Shindo, E., Mizuta, R., Obata, A., Adachi, Y., & Ishii, M. (2019). The Meteorological Research Institute Earth System Model Version 2.0, MRI-ESM2.0: Description and Basic Evaluation of the Physical Component. *Journal of the Meteorological Society of Japan. Ser. II*, *97*(5), 931–965. https://doi.org/10.2151/JMSJ.2019-051

Zhang, H., Zhang, M., Jin, J., Fei, K., Ji, D., Wu, C., Zhu, J., He, J., Chai, Z., Xie, J., Dong, X., Zhang, D., Bi, X., Cao, H., Chen, H., Chen, K., Chen, X., Gao, X., Hao, H., … Zhu, J. (2020). Description and Climate Simulation Performance of CAS-ESM Version 2. *Journal of Advances in Modeling Earth Systems*, *12*(12), e2020MS002210. https://doi.org/10.1029/2020MS002210

Ziehn, T., Chamberlain, M. A., Law, R. M., Lenton, A., Bodman, R. W., Dix, M., Stevens, L., Wang, Y. P., & Srbinovsky, J. (2020). The Australian Earth System Model: ACCESS-ESM1.5. *Journal of Southern Hemisphere Earth Systems Science*, *70*(1), 193–214. https://doi.org/10.1071/ES19035

Ziehn, T., Lenton, A., Law, R. M., Matear, R. J., & Chamberlain, M. A. (2017). The carbon cycle in the Australian Community Climate and Earth System Simulator (ACCESS-ESM1) - Part 2: Historical simulations. *Geoscientific Model Development*, *10*(7), 2591–2614. https://doi.org/10.5194/GMD-10-2591-2017

Moat, B. I., Frajka-Williams, E., Smeed, D. A., Rayner, D., Johns, W. E., Baringer, M. O., et al. (2022). Atlantic meridional overturning circulation observed by the RAPID-MOCHA-WBTS (RAPID-Meridional Overturning Circulation and Heatflux Array-Western Boundary Time Series) array at 26N from 2004 to 2020 (v2020.2). [Dataset]. British Oceanographic Data Centre, Natural Environment Research Council. https://doi.org/10.5285/e91b10af-6f0a-7fa7-e053-6c86abc05a09